Combustion, Explosion, and Shock Waves, Vol. 45, No. 6, pp. 635–645, 2009

Comparative Study of the Influence of CO_2 and H_2O on the Chemical Structure of Lean and Rich Methane–Air Flames at Atmospheric Pressure

A. Matynia,[1] J.-L. Delfau,[1] L. Pillier,[1] and C. Vovelle[1]

UDC 536.46

Translated from *Fizika Goreniya i Vzryva*, Vol. 45, No. 6, pp. 3–14, November–December, 2009.
Original article submitted November 11, 2008.

A comparative study of the influence of CO_2 and H_2O on both lean and rich CH_4–air laminar flames is performed. Six premixed flames are stabilized on a flat flame burner at atmospheric pressure: lean (with the equivalence ratio maintained constant at $\phi = 0.7$) and rich (with the equivalence ratio maintained constant at $\phi = 1.4$) CH_4–air, CH_4–CO_2–air, and CH_4–H_2O–air flames. These flames are studied experimentally and numerically. The $[CO_2]/[CH_4]$ and $[H_2O]/[CH_4]$ ratios are kept equal to 0.4 for both flames series. Species mole fraction profiles are measured by gas chromatography and Fourier transform infrared spectroscopy analyses of gas samples withdrawn along the vertical axis by a quartz microprobe. Flames structures are computed by using the ChemkinII/Premix code. Four detailed combustion mechanisms are used to calculate the laminar flame velocities and species mole fraction profiles: GRI-Mech 3.0, Dagaut, UCSD, and GDFkin®3.0.

Key words: methane–air flames, chemical structure, CO_2 and H_2O additives, atmospheric pressure.

INTRODUCTION

Exhaust gas recirculation (EGR) is one of the most effective techniques currently available for reducing NO_x emissions from engines. The principle is recirculation of a portion of the engine exhaust gas back to the engine cylinders. Intermixing of the incoming air with the recirculated exhaust gas dilutes the mixture with an inert gas, lowering the adiabatic flame temperature and NO_x emissions by the reduction of the rate of production of "thermal" NO_x. The exhaust gas is mainly composed of CO_2, N_2, H_2O, and O_2. Studies on the EGR effect on combustion chemistry are usually performed with addition of a simulated exhaust gas containing a mixture of CO_2 and N_2 [1–3], a significant water content in the real exhaust gas being ignored. Only few studies exist on the effect of water, as it is usually difficult to add water (vapor) to testing combustion chambers.

Ren et al. [4, 5] studied the influence of H_2, CO, CO_2, and H_2O additives in lean premixed methane–air flames (separately and in combination) on NO_x reduction, laminar flame speeds, and extinction. Addition of CO_2 and H_2O was demonstrated to decrease NO_x emissions, the decrease being larger when the equivalence ratio increased. The presence of CO_2 and H_2O in the fuel mixture results in reduction of the laminar flame speed and extinction strain rate. Renard et al. [6] studied the effect of CO_2 and H_2O addition on hydrocarbon intermediates in rich C_2H_4–O_2–Ar flames and concluded that a larger hydroxyl radical production is responsible for reduction of hydrocarbon intermediates in the added flames. Zhao et al. [7] and Hwang et al. [8] performed numerical studies on the effect of H_2O addition to CH_4–O_2–N_2 diffusion flames.

In a previous work [9], we studied both experimentally and numerically the influence of CO_2 and $CO_2 + H_2$ addition on the chemical structure of a lean premixed CH_4–air flame (equivalence ratio $\phi = 0.7$). The objective was linked to the potential use of biogas

[1]Institut de Combustion, Aérothermique, Réactivité, Environnement, 45071 Orléans, France; pillier@cnrs-orleans.fr.

TABLE 1
Initial Conditions of the Lean and Rich CH_4–Air, CH_4–CO_2–Air, and CH_4–H_2O–Air Flames ($p = 1$ atm and $T_0 = 298$ K)

Flame	Mole fractions				ϕ	Mass flux, $g \cdot cm^{-2} \cdot sec^{-1}$
	CH_4	CO_2	H_2O	air		
1a (CH_4–air)	0.0683	—	—	0.9317	0.7	0.0240
2a (CH_4–CO_2–air)	0.0665	0.0266	—	0.9069	0.7	0.0192
3a (CH_4–H_2O–air)	0.0665	—	0.0266	0.9069	0.7	0.0186
1b (CH_4–air)	0.1279	—	—	0.8721	1.4	0.0234
2b (CH_4–CO_2–air)	0.1217	0.0487	—	0.8296	1.4	0.0103
3b (CH_4–H_2O–air)	0.1217	—	0.0487	0.8296	1.4	0.0163

generated by biomass to reduce NO_x formation. The presence of CO_2 in the biogas, however, decreases the burning velocity and, hence, the energy conversion efficiency. Addition of H_2 was considered as a way to increase the burning velocity and limit the negative effect of CO_2. The $[CO_2/CH_4]$ ratio was fixed at 0.4. In the present work, we kept the same ratio to complement our previous work and study the influence of CO_2 and H_2O addition on the chemical structure of both lean and rich premixed CH_4–air flames stabilized at atmospheric pressure. Experimental measurements were performed by methods of gas chromatography (GC) and Fourier transform infrared spectroscopy (FTIR). Flame structures were computed on the basis of the ChemkinII/Premix code and four detailed combustion mechanisms [10–13].

EXPERIMENT

Six premixed flames were stabilized on a flat flame burner at atmospheric pressure and were studied experimentally and numerically: three lean flames with the equivalence ratio maintained constant at $\phi = 0.7$ [CH_4–air (flame 1a), CH_4–CO_2–air (flame 2a), and CH_4–H_2–air (flame 3a)], and three rich flames with the equivalence ratio maintained at $\phi = 1.4$ [CH_4–air (flame 1b), CH_4–CO_2–air (flame 2b), and CH_4–H_2O–air (flame 3b)]. The $[CO_2]/[CH_4]$ and $[H_2O]/[CH_4]$ ratios were kept equal to 0.4 for both flames series. The burner was made of a brass disc with small holes (0.7 mm in diameter) drilled on a circular area 4 cm in diameter. A perforated plate was located at 1 cm above the burner surface to reduce heat exchanges between the flame and the burner and to stabilize the flame. CH_4 and CO_2 from compressed pure gas cylinders were premixed with air prior to entering the burner. Water was injected by a peristaltic pump, became then vaporized, and finally mixed with CH_4 and air. The pipes and the burner were heated to avoid water re-condensation. Table 1 lists the initial conditions for the six flames studied.

Gas samples were withdrawn along the axis of symmetry of the flame by a quartz microprobe constructed from a quartz tube (0.5 cm in diameter) drawn to a cone at the end. A hole (0.1 mm in diameter) was drilled at the tip of this cone. The gaseous samples withdrawn from the flame were analyzed either by GC or by FTIR. For GC analyses, the gaseous samples where stored in Pyrex flasks at a low pressure ($\leqslant$2.0 kPa) and were compressed by a home-made piston up to 53 kPa prior to injection into the chromatograph. The gaseous samples were collected directly in the FTIR cell up to 3.3 kPa. Species analyzed by GC were CH_4, C_2H_4, C_2H_2, C_2H_6, C_3H_8, C_3H_6, CO, CO_2, H_2O, H_2, O_2, and N_2. CH_2O was measured by FTIR. Two GC systems were used for the analyses. The first one, with a thermal conductivity detector (TCD) and a flame ionization detector (FID), was kitted out with two capillaries columns: Poraplot Q and Molecular Sieve (MS5A). The second chromatograph operated with FID and was used for separation of CH_4 and C_2 intermediates on an Al_2O_3/KCl column. Helium was used as a carrier gas for all species analyses, except for H_2, which was measured with nitrogen to enhance the detector sensitivity. Species calibrations were

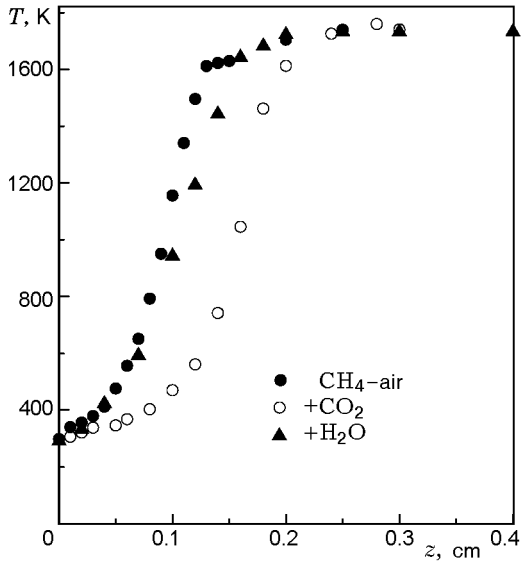

Fig. 1. Temperature profiles used as input data in lean flame simulations ($\phi = 0.7$).

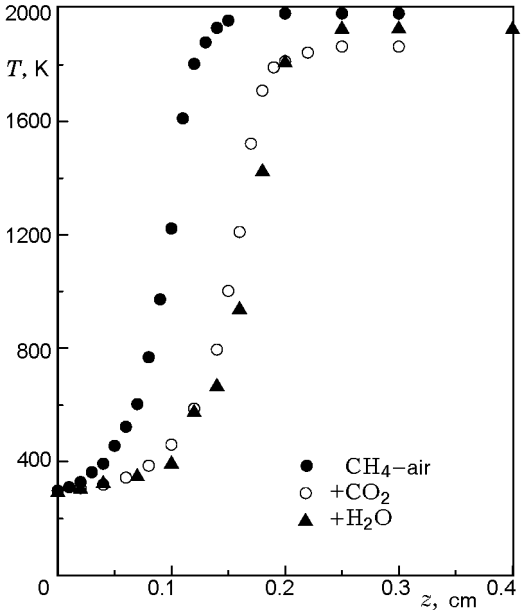

Fig. 2. Temperature profiles used as input data in rich flame simulations ($\phi = 1.4$).

TABLE 2

Comparison of Measured and Computed Species Mole Fractions in Flame 1a (CH_4–Air; $\phi = 0.7$)

Mole fractions X at a distance z		Experiment	GRI-Mech 3.0	UCSD	Dagaut	GDFkin®3.0
CH_4	X_i $(z = 0)$	$6.28 \cdot 10^{-2}$	$6.80 \cdot 10^{-2}$	$6.65 \cdot 10^{-2}$	$6.79 \cdot 10^{-2}$	$6.79 \cdot 10^{-2}$
	z $(X_i = X_{i,\mathrm{med}})$, cm	0.09	0.08	0.08	0.08	0.08
O_2	$X_{i,0}$ $(z = 0)$	$1.84 \cdot 10^{-1}$	$1.95 \cdot 10^{-1}$	$1.94 \cdot 10^{-1}$	$1.95 \cdot 10^{-1}$	$1.95 \cdot 10^{-1}$
	$X_{i,f}$ $(z = 0.3$ cm$)$	$6.36 \cdot 10^{-2}$	$6.02 \cdot 10^{-2}$	$6.00 \cdot 10^{-2}$	$6.03 \cdot 10^{-2}$	$6.00 \cdot 10^{-2}$
	z $(X_i = X_{i,\mathrm{med}})$, cm	0.10	0.09	0.08	0.10	0.09
CO_2	$X_{i,f}$ $(z = 0.3$ cm$)$	$6.56 \cdot 10^{-2}$	$6.63 \cdot 10^{-2}$	$6.58 \cdot 10^{-2}$	$6.60 \cdot 10^{-2}$	$6.61 \cdot 10^{-2}$
	z $(X_i = X_{i,\mathrm{med}})$, cm	0.12	0.11	0.10	0.11	0.11
H_2O	$X_{i,f}$ $(z = 0.3$ cm$)$	$1.47 \cdot 10^{-1}$	$1.34 \cdot 10^{-1}$	$1.33 \cdot 10^{-1}$	$1.33 \cdot 10^{-1}$	$1.33 \cdot 10^{-1}$
	z $(X_i = X_{i,\mathrm{med}})$, cm	0.11	0.08	0.08	0.09	0.08
CO	$X_{i,\max}$	$1.80 \cdot 10^{-2}$	$2.25 \cdot 10^{-2}$	$2.27 \cdot 10^{-2}$	$2.07 \cdot 10^{-2}$	$2.10 \cdot 10^{-2}$
	z $(X_i = X_{i,\max})$, cm	0.12	0.11	0.10	0.11	0.11
H_2	$X_{i,\max}$	$5.05 \cdot 10^{-3}$	$4.81 \cdot 10^{-3}$	$4.00 \cdot 10^{-3}$	$4.39 \cdot 10^{-3}$	$4.23 \cdot 10^{-3}$
	z $(X_i = X_{i,\max})$, cm	0.11	0.10	0.10	0.11	0.11
C_2H_6	$X_{i,\max}$	$4.22 \cdot 10^{-4}$	$3.75 \cdot 10^{-4}$	$6.79 \cdot 10^{-4}$	$7.65 \cdot 10^{-4}$	$8.33 \cdot 10^{-4}$
	z $(X_i = X_{i,\max})$, cm	0.11	0.09	0.08	0.10	0.09
C_2H_4	$X_{i,\max}$	$2.31 \cdot 10^{-4}$	$1.96 \cdot 10^{-4}$	$4.83 \cdot 10^{-4}$	$5.00 \cdot 10^{-4}$	$5.51 \cdot 10^{-4}$
	z $(X_i = X_{i,\max})$, cm	0.11	0.10	0.09	0.10	0.10
C_2H_2	$X_{i,\max}$	$3.54 \cdot 10^{-5}$	$8.59 \cdot 10^{-6}$	$2.17 \cdot 10^{-5}$	$3.43 \cdot 10^{-5}$	$3.11 \cdot 10^{-5}$
	z $(X_i = X_{i,\max})$, cm	0.12	0.10	0.09	0.11	0.11
NO	$X_{i,f}$ $(z = 0.3$ cm$)$	—	$5.12 \cdot 10^{-6}$	—	—	$4.94 \cdot 10^{-6}$
	z $(X_i = X_{i,\mathrm{med}})$, cm	—	0.12	—	—	0.12

TABLE 3

Comparison of Measured and Computed Species Mole Fractions in Flame 2a (CH_4–CO_2–Air; $\phi = 0.7$)

Mole fractions X at a distance z		Experiment	GRI-Mech 3.0	UCSD	Dagaut	GDFkin®3.0
CH_4	X_i ($z = 0$)	$6.34 \cdot 10^{-2}$	$6.59 \cdot 10^{-2}$	$6.61 \cdot 10^{-2}$	$6.60 \cdot 10^{-2}$	$6.57 \cdot 10^{-2}$
	z ($X_i = X_{i,\mathrm{med}}$), cm	0.13	0.13	0.12	0.14	0.14
O_2	$X_{i,0}$ ($z = 0$)	$1.80 \cdot 10^{-1}$	$1.90 \cdot 10^{-1}$	$1.90 \cdot 10^{-1}$	$1.90 \cdot 10^{-1}$	$1.90 \cdot 10^{-1}$
	$X_{i,f}$ ($z = 0.3$ cm)	$6.45 \cdot 10^{-2}$	$5.87 \cdot 10^{-2}$	$5.90 \cdot 10^{-2}$	$5.85 \cdot 10^{-2}$	$5.96 \cdot 10^{-2}$
	z ($X_i = X_{i,\mathrm{med}}$), cm	0.14	0.14	0.14	0.15	0.16
CO_2	$X_{i,0}$ ($z = 0$)	$2.74 \cdot 10^{-2}$	$2.67 \cdot 10^{-2}$	$2.67 \cdot 10^{-2}$	$2.67 \cdot 10^{-2}$	$2.67 \cdot 10^{-2}$
	$X_{i,f}$ ($z = 0.3$ cm)	$9.39 \cdot 10^{-2}$	$9.06 \cdot 10^{-2}$	$8.94 \cdot 10^{-2}$	$9.05 \cdot 10^{-2}$	$8.96 \cdot 10^{-2}$
	z ($X_i = X_{i,\mathrm{med}}$), cm	0.15	0.16	0.15	0.17	0.17
H_2O	$X_{i,f}$ ($z = 0.3$ cm)	$1.47 \cdot 10^{-1}$	$1.30 \cdot 10^{-1}$	$1.30 \cdot 10^{-1}$	$1.30 \cdot 10^{-1}$	$1.29 \cdot 10^{-1}$
	z ($X_i = X_{i,\mathrm{med}}$), cm	0.14	0.13	0.13	0.14	0.15
CO	$X_{i,\max}$	$1.60 \cdot 10^{-2}$	$2.08 \cdot 10^{-2}$	$2.16 \cdot 10^{-2}$	$1.92 \cdot 10^{-2}$	$1.91 \cdot 10^{-2}$
	z ($X_i = X_{i,\max}$), cm	0.15	0.16	0.16	0.17	0.18
H_2	$X_{i,\max}$	$2.82 \cdot 10^{-3}$	$4.13 \cdot 10^{-3}$	$3.60 \cdot 10^{-3}$	$3.79 \cdot 10^{-3}$	$3.55 \cdot 10^{-3}$
	z ($X_i = X_{i,\max}$), cm	0.18	0.15	0.15	0.16	0.17
C_2H_6	$X_{i,\max}$	$3.23 \cdot 10^{-4}$	$3.47 \cdot 10^{-4}$	$6.35 \cdot 10^{-4}$	$7.06 \cdot 10^{-4}$	$7.53 \cdot 10^{-4}$
	z ($X_i = X_{i,\max}$), cm	0.15	0.14	0.13	0.15	0.16
C_2H_4	$X_{i,\max}$	$1.80 \cdot 10^{-4}$	$2.00 \cdot 10^{-4}$	$4.68 \cdot 10^{-4}$	$4.85 \cdot 10^{-4}$	$5.27 \cdot 10^{-4}$
	z ($X_i = X_{i,\max}$), cm	0.15	0.15	0.14	0.16	0.17
C_2H_2	$X_{i,\max}$	$2.48 \cdot 10^{-5}$	$7.93 \cdot 10^{-6}$	$2.03 \cdot 10^{-5}$	$3.06 \cdot 10^{-5}$	$2.62 \cdot 10^{-5}$
	z ($X_i = X_{i,\max}$), cm	0.15	0.16	0.15	0.17	0.18
NO	$X_{i,f}$ ($z = 0.3$ cm)	—	$3.57 \cdot 10^{-6}$	—	—	$3.63 \cdot 10^{-6}$
	z ($X_i = X_{i,\mathrm{med}}$), cm	—	0.167	—	—	0.17

performed by using gaseous mixtures of known compositions. The accuracy was estimated to be ±5% for the permanent gases and C_1 and C_2 hydrocarbons, ±10% for H_2O, and ±20% for CH_2O. These deviations correspond to the inaccuracies resulting from sampling pressure measurements and GC or FTIR reproducibility.

The temperature of the burnt gases was measured in each flame by a Pt/(Pt–10%Rh) thermocouple constructed with thin wires (50 μm in diameter) tightened parallel to the burner surface and coated with a BeO–Y_2O_3 deposit to reduce catalytic effects [14]. The measured temperatures were increased by 12% to compensate radiative heat losses. This factor was determined in previous experiments [15] where heat losses were measured by means of the electrical compensation technique [16]. Visual observations showed that locating the thermocouple in the luminous flame front induced a noticeable flame displacement. Hence, to measure the temperature through the flame zone, the sampling probe was used as a pneumatic temperature-measuring device by determining the rate of gas inflow into a known volume as a function of the probe position in the flame. This technique had been previously used by Kaiser et al. [17] and details of the method had been given in their paper.

MODELING

The flames structures were computed by using the Chemkin II [18] and Premix [19] codes. Four detailed combustion mechanisms were used to simulate the laminar flame velocities, temperatures, and species mole fraction profiles. The GRI-Mech 3.0 mechanism [10] includes 53 species and 325 reversible reactions. The mechanism developed by Dagaut et al. [11] contains 54 species involved into 281 reactions (277 reversible and 4 irreversible). The 2005 version of the mechanism developed at the University of California, San Diego [12] (UCSD) contains 40 species (up to C_3) and 175 reversible reactions. Finally, the GDFkin®3.0 mechanism, developed by El Bakali et al. [13], contains 121 species and 884 reversible reactions. The GRI-Mech 3.0 and GDFkin®3.0 mechanisms contain their own NO_x chemistry sub-mechanisms, whereas the UCSD mechanism

TABLE 4

Comparison of Measured and Computed Species Mole Fraction in Flame 3a (CH_4–H_2O–Air; $\phi = 0.7$)

Mole fractions X at a distance z		Experiment	GRI-Mech 3.0	UCSD	Dagaut	GDFkin®3.0
CH_4	X_i ($z = 0$)	$6.05 \cdot 10^{-2}$	$6.39 \cdot 10^{-2}$	$6.41 \cdot 10^{-2}$	$6.37 \cdot 10^{-2}$	$6.40 \cdot 10^{-2}$
	z ($X_i = X_{i,\mathrm{med}}$), cm	0.10	0.09	0.09	0.09	0.09
O_2	$X_{i,0}$ ($z = 0$)	$1.64 \cdot 10^{-1}$	$1.89 \cdot 10^{-1}$	$1.89 \cdot 10^{-1}$	$1.89 \cdot 10^{-1}$	$1.89 \cdot 10^{-1}$
	$X_{i,f}$ ($z = 0.3$ cm)	$6.39 \cdot 10^{-2}$	$5.90 \cdot 10^{-2}$	$5.89 \cdot 10^{-2}$	$5.90 \cdot 10^{-2}$	$5.87 \cdot 10^{-2}$
	z ($X_i = X_{i,\mathrm{med}}$), cm	0.11	0.10	0.09	0.10	0.10
CO_2	$X_{i,f}$ ($z = 0.3$ cm)	$6.44 \cdot 10^{-2}$	$6.46 \cdot 10^{-2}$	$6.44 \cdot 10^{-2}$	$6.44 \cdot 10^{-2}$	$6.47 \cdot 10^{-2}$
	z ($X_i = X_{i,\mathrm{med}}$), cm	0.12	0.11	0.11	0.12	0.12
H_2O	$X_{i,0}$ ($z = 0$)	$3.21 \cdot 10^{-2}$	$2.98 \cdot 10^{-2}$	$2.95 \cdot 10^{-2}$	$3.02 \cdot 10^{-2}$	$2.95 \cdot 10^{-2}$
	$X_{i,f}$ ($z = 0.3$ cm)	$1.53 \cdot 10^{-1}$	$1.57 \cdot 10^{-1}$	$1.57 \cdot 10^{-1}$	$1.57 \cdot 10^{-1}$	$1.57 \cdot 10^{-1}$
	z ($X_i = X_{i,\mathrm{med}}$), cm	0.11	0.09	0.09	0.10	0.09
CO	$X_{i,\max}$	$1.33 \cdot 10^{-2}$	$2.00 \cdot 10^{-2}$	$2.09 \cdot 10^{-2}$	$1.84 \cdot 10^{-2}$	$1.87 \cdot 10^{-2}$
	z ($X_i = X_{i,\max}$), cm	0.14	0.12	0.11	0.12	0.12
H_2	$X_{i,\max}$	$3.14 \cdot 10^{-3}$	$4.32 \cdot 10^{-3}$	$3.86 \cdot 10^{-3}$	$4.00 \cdot 10^{-3}$	$3.86 \cdot 10^{-3}$
	z ($X_i = X_{i,\max}$), cm	0.12	0.11	0.11	0.11	0.11
C_2H_6	$X_{i,\max}$	$2.64 \cdot 10^{-4}$	$3.49 \cdot 10^{-4}$	$6.40 \cdot 10^{-4}$	$7.03 \cdot 10^{-4}$	$7.74 \cdot 10^{-4}$
	z ($X_i = X_{i,\max}$), cm	0.11	0.10	0.09	0.10	0.10
C_2H_4	$X_{i,\max}$	$1.47 \cdot 10^{-4}$	$2.09 \cdot 10^{-4}$	$4.77 \cdot 10^{-4}$	$4.91 \cdot 10^{-4}$	$5.48 \cdot 10^{-4}$
	z ($X_i = X_{i,\max}$), cm	0.11	0.10	0.10	0.11	0.11
C_2H_2	$X_{i,\max}$	$1.97 \cdot 10^{-5}$	$9.30 \cdot 10^{-6}$	$2.15 \cdot 10^{-5}$	$3.40 \cdot 10^{-5}$	$3.06 \cdot 10^{-5}$
	z ($X_i = X_{i,\max}$), cm	0.14	0.12	0.11	0.12	0.12
NO	$X_{i,f}$ ($z = 0.3$ cm)	—	$3.68 \cdot 10^{-6}$	—	—	$4.07 \cdot 10^{-6}$
	z ($X_i = X_{i,\mathrm{med}}$), cm	—	0.13	—	—	0.13

and the version of the Dagaut's mechanism that was used do not include NO_x chemistry.

Thermodynamic and transport data were taken without any changes from the respective mechanisms. Flame simulations were performed both with "BURN" and "FREE" options. Very closed results were obtained for the species mole fraction profiles in both cases. While additional information on both the burning rate and the adiabatic temperature were obtained when the "FREE" option was used, all computed results presented here refer to free flame simulations performed with the experimental temperature profiles introduced as a starting estimate.

RESULTS AND DISCUSSION

Influence of CO_2 and H_2O on the Species Mole Fraction Profiles

Figures 1 and 2 display the temperature profiles used as input data in the Premix code to simulate the structure of the lean and rich flames, respectively. Both flames are shifted downstream when CO_2 is added to the fresh gas mixture. Addition of H_2O to the rich flame produces a similar shift, whereas the position of the lean flame front is almost unaffected.

Tables 2–4 compare the measured and computed mole fractions for three lean flames. The results obtained for the rich flames are summarized in Tables 5–7. In these tables, we use $X_{i,\mathrm{med}} = X_{i0} + (X_{i,f} - X_{i0})/2$, where X_{i0} is the mole fraction at the burner surface and $X_{i,f}$ is the mole fraction in the burnt gases. In this work, $X_{i,f}$ was systematically measured at a distance $z = 0.3$ cm from the burner surface. The position of this central part of the mole fraction gradient ($X_{i,\mathrm{med}}$) was also considered to check the accuracy of model predictions for the reactants and the final products. The maximum mole fraction ($X_{i,\max}$) and its location in the flame front (z) were considered as a comparison criteria for the intermediate species.

Lean Flames. In lean flames, the four mechanisms predicted the mole fraction profiles for the reactants (CH_4 and O_2) and the final products (CO_2 and H_2O), which are both very close to each other and

TABLE 5

Comparison of Measured and Computed Species Mole Fractions in Flame 1b (CH_4–Air; $\phi = 1.4$)

Mole fractions X at a distance z		Experiment	GRI-Mech 3.0	UCSD	Dagaut	GDFkin®3.0
CH_4	X_i ($z = 0$)	$1.11 \cdot 10^{-1}$	$1.24 \cdot 10^{-1}$	$1.24 \cdot 10^{-1}$	$1.27 \cdot 10^{-1}$	$1.27 \cdot 10^{-1}$
	z ($X_i = X_{i,\mathrm{med}}$), cm	0.09	0.11	0.11	0.09	0.10
O_2	$X_{i,0}$ ($z = 0$)	$1.65 \cdot 10^{-1}$	$1.81 \cdot 10^{-1}$	$1.82 \cdot 10^{-1}$	$1.82 \cdot 10^{-1}$	$1.82 \cdot 10^{-1}$
	$X_{i,f}$ ($z = 0.3$ cm)	$1.02 \cdot 10^{-2}$	$1.87 \cdot 10^{-5}$	$3.52 \cdot 10^{-5}$	$4.12 \cdot 10^{-5}$	$2.17 \cdot 10^{-5}$
	z ($X_i = X_{i,\mathrm{med}}$), cm	0.10	0.12	0.12	0.10	0.11
CO_2	$X_{i,f}$ ($z = 0.3$ cm)	$5.10 \cdot 10^{-2}$	$4.63 \cdot 10^{-2}$	$4.57 \cdot 10^{-2}$	$4.78 \cdot 10^{-2}$	$4.58 \cdot 10^{-2}$
	z ($X_i = X_{i,\mathrm{med}}$), cm	0.11	0.14	0.14	0.11	0.13
H_2O	$X_{i,f}$ ($z = 0.3$ cm)	$1.63 \cdot 10^{-1}$	$1.77 \cdot 10^{-1}$	$1.78 \cdot 10^{-1}$	$1.75 \cdot 10^{-1}$	$1.75 \cdot 10^{-1}$
	z ($X_i = X_{i,\mathrm{med}}$), cm	0.09	0.11	0.11	0.09	0.10
CO	$X_{i,f}$ ($z = 0.3$ cm)	$7.19 \cdot 10^{-2}$	$7.10 \cdot 10^{-2}$	$7.14 \cdot 10^{-2}$	$6.94 \cdot 10^{-2}$	$7.08 \cdot 10^{-2}$
	z ($X_i = X_{i,\mathrm{med}}$), cm	0.10	0.12	0.12	0.09	0.10
H_2	$X_{i,f}$ ($z = 0.3$ cm)	$6.12 \cdot 10^{-2}$	$6.16 \cdot 10^{-2}$	$6.13 \cdot 10^{-2}$	$6.18 \cdot 10^{-2}$	$6.31 \cdot 10^{-2}$
	z ($X_i = X_{i,\mathrm{med}}$), cm	0.08	0.10	0.10	0.07	0.08
C_2H_6	$X_{i,\max}$	$1.29 \cdot 10^{-3}$	$1.37 \cdot 10^{-3}$	$1.43 \cdot 10^{-3}$	$2.20 \cdot 10^{-3}$	$2.29 \cdot 10^{-3}$
	z ($X_i = X_{i,\max}$)	0.11	0.12	0.13	0.09	0.11
C_2H_4	$X_{i,\max}$	$1.62 \cdot 10^{-3}$	$1.84 \cdot 10^{-3}$	$2.58 \cdot 10^{-3}$	$2.59 \cdot 10^{-3}$	$3.05 \cdot 10^{-3}$
	z ($X_i = X_{i,\max}$)	0.11	0.13	0.13	0.10	0.12
C_2H_2	$X_{i,\max}$	$2.45 \cdot 10^{-3}$	$1.75 \cdot 10^{-3}$	$2.09 \cdot 10^{-3}$	$2.00 \cdot 10^{-3}$	$2.26 \cdot 10^{-3}$
	z ($X_i = X_{i,\max}$)	0.12	0.16	0.16	0.12	0.14
NO	$X_{i,f}$ ($z = 0.3$ cm)	—	$4.58 \cdot 10^{-5}$	—	—	$7.83 \cdot 10^{-5}$
	z ($X_i = X_{i,\mathrm{med}}$), cm	—	0.19	—	—	0.15

in good agreement with the experiments. CO and H_2 are the main intermediate species in lean flames; their predicted maximum mole fractions are roughly similar and in reasonable agreement with the experiments. For CO, the slight evolution $X_{\mathrm{CO,max}}$ (flame 1a) > $X_{\mathrm{CO,max}}$ (flame 2a) > $X_{\mathrm{CO,max}}$ (flame 3a) observed experimentally is also reproduced by the four mechanisms. For H_2, addition of CO_2 or H_2O reduces the experimental maximum mole fraction with respect to the methane–air flame, but the maximum measured in flame 3a is higher than that in flame 2a. The four mechanisms lead to similar evolutions.

C_2 species are minor intermediates in these lean flames, and some scatter is observed in the computed values. The GRI-Mech 3.0 mechanism predicts the maximum concentration of C_2H_6 and C_2H_4 in all lean flames with reasonable accuracy. On the other hand, it underpredicts markedly the maximum C_2H_2 mole fraction. The Dagaut, UCSD, and GDFkin®3.0 mechanisms overpredict the C_2H_6 and C_2H_4 maximum mole fractions; however, they ensure better agreement with the experiments for C_2H_2. The NO mole fractions calculated with the GRI-Mech 3.0 and the GDFkin®3.0 mechanisms are approximately identical in the burnt gases. It is seen from Tables 2–4 that addition of CO_2 and H_2O reduces the NO mole fraction by 28% and 23%, respectively.

Concerning the relative positions z of the maximum mole fraction gradients (for reactants and final products) or of the maximum mole fractions (for intermediates), the four mechanisms predict values that are almost identical and in good agreement with the experiments.

Rich Flames. In rich flames (Tables 5–7), the final products include CO and H_2 in addition to CO_2 and H_2O. Good agreement with the experiments is observed with the four mechanisms for the final mole fractions reached in the burnt gases. Tables 5 and 6 show that CO_2 addition slightly increases the final CO mole fraction and decreases markedly the H_2 mole fractions. Addition of H_2O produces only slight variations of the CO and H_2 final mole fractions. The former decreases, whereas the latter increases.

In rich flames, C_2 species are important intermediates with the maximum concentrations far larger than those in lean flames. In three rich flames, the exper-

TABLE 6

Comparison of Measured and Computed Species Mole Fractions in Flame 2b (CH_4–CO_2–Air; $\phi = 1.4$)

Mole fractions X at a distance z		Experiment	GRI-Mech 3.0	UCSD	Dagaut	GDFkin®3.0
CH_4	X_i $(z = 0)$	$1.12 \cdot 10^{-1}$	$1.20 \cdot 10^{-1}$	$1.21 \cdot 10^{-1}$	$1.21 \cdot 10^{-1}$	$1.19 \cdot 10^{-1}$
	z $(X_i =_{i,\mathrm{med}})$, cm	0.15	0.19	0.18	0.15	0.16
O_2	$X_{i,0}$ $(z = 0)$	$1.70 \cdot 10^{-1}$	$1.73 \cdot 10^{-1}$	$1.73 \cdot 10^{-1}$	$1.73 \cdot 10^{-1}$	$1.72 \cdot 10^{-1}$
	$X_{i,f}$ $(z = 0.3$ cm$)$	$1.16 \cdot 10^{-2}$	$1.75 \cdot 10^{-4}$	$1.67 \cdot 10^{-3}$	$7.00 \cdot 10^{-5}$	$1.03 \cdot 10^{-4}$
	z $(X_i = X_{i,\mathrm{med}})$, cm	0.15	0.14	0.19	0.16	0.18
CO_2	$X_{i,0}$ $(z = 0)$	$4.57 \cdot 10^{-2}$	$4.87 \cdot 10^{-2}$	$4.87 \cdot 10^{-2}$	$4.86 \cdot 10^{-2}$	$4.88 \cdot 10^{-2}$
	$X_{i,f}$ $(z = 0.3$ cm$)$	$8.53 \cdot 10^{-2}$	$7.55 \cdot 10^{-2}$	$7.61 \cdot 10^{-2}$	$7.96 \cdot 10^{-2}$	$7.90 \cdot 10^{-2}$
	z $(X_i = X_{i,\mathrm{med}})$, cm	0.16	0.22	0.21	0.18	0.19
H_2O	$X_{i,f}$ $(z = 0.3$ cm$)$	$1.81 \cdot 10^{-1}$	$1.80 \cdot 10^{-1}$	$1.82 \cdot 10^{-1}$	$1.79 \cdot 10^{-1}$	$1.80 \cdot 10^{-1}$
	z $(X_i = X_{i,\mathrm{med}})$, cm	0.15	0.19	0.18	0.16	0.16
CO	$X_{i,f}$ $(z = 0.3$ cm$)$	$7.65 \cdot 10^{-2}$	$7.82 \cdot 10^{-2}$	$7.93 \cdot 10^{-2}$	$7.82 \cdot 10^{-2}$	$7.85 \cdot 10^{-2}$
	z $(X_i = X_{i,\mathrm{med}})$, cm	0.15	0.20	0.19	0.16	0.18
H_2	$X_{i,f}$ $(z = 0.3$ cm$)$	$4.45 \cdot 10^{-2}$	$4.37 \cdot 10^{-2}$	$4.45 \cdot 10^{-2}$	$4.71 \cdot 10^{-2}$	$4.64 \cdot 10^{-2}$
	z $(X_i = X_{i,\mathrm{med}})$, cm	0.14	0.16	0.16	0.13	0.14
C_2H_6	$X_{i,\max}$	$1.22 \cdot 10^{-3}$	$1.12 \cdot 10^{-3}$	$1.18 \cdot 10^{-3}$	$1.81 \cdot 10^{-3}$	$1.88 \cdot 10^{-3}$
	z $(X_i = X_{i,\max})$	0.16	0.22	0.20	0.16	0.19
C_2H_4	$X_{i,\max}$	$1.47 \cdot 10^{-3}$	$1.77 \cdot 10^{-3}$	$2.34 \cdot 10^{-3}$	$2.30 \cdot 10^{-3}$	$2.62 \cdot 10^{-3}$
	z $(X_i = X_{i,\max})$	0.16	0.23	0.22	0.18	0.20
C_2H_2	$X_{i,\max}$	$1.77 \cdot 10^{-3}$	$1.57 \cdot 10^{-3}$	$8.52 \cdot 10^{-4}$	$1.65 \cdot 10^{-3}$	$1.68 \cdot 10^{-3}$
	z $(X_i = X_{i,\max})$	0.17	0.27	0.25	0.20	0.23
NO	$X_{i,f}$ $(z = 0.3$ cm$)$	—	$9.83 \cdot 10^{-6}$	—	—	$3.23 \cdot 10^{-5}$
	z $(X_i = X_{i,\mathrm{med}})$, cm	—	0.25	—	—	0.21

iments provided the C_2 species maximum mole fractions ranging as $X_{C_2H_2} > X_{C_2H_4} > X_{C_2H_6}$. GRI-Mech 3.0 predicts the same order in the CH_4–H_2O–air flame (see Table 7) but not in the CH_4–air and CH_4–CO_2–air flames where $X_{C_2H_4} > X_{C_2H_2}$. The three other mechanisms also predict $X_{C_2H_4} > X_{C_2H_2}$. When the changes induced by CO_2 or H_2 addition are considered, the UCSD and Dagaut mechanisms reproduce the experimental observations more closely. Both additives decrease the maximum mole fractions of C_2H_4 and C_2H_2, and this effect is more pronounced when CO_2 is added to the flame. Calculations of NO mole fractions with the GRI-Mech 3.0 and GDFkin®3.0 mechanisms lead to different results with higher values predicted by GDFkin®3.0. The results show a significant reduction of the NO mole fraction due to addition of CO_2 (reduction of 78% for the GRI-Mech 3.0 and 58% for GDFkin®3.0) and H_2O (reduction of 77% for the GRI-Mech 3.0 and 54% for GDFkin®3.0).

From comparisons of computed and measured species mole fraction profiles, it can be concluded that the four mechanisms predict the evolution of the major species rather well, but lead to discrepancies for the minor intermediates.

Influence of CO_2 and H_2O on Flame Velocity and Maximum Temperature

Table 8 compares the calculated laminar flame velocities for six flames studied. Some scatters are observed between the four mechanisms. Relative variations induced by CO_2 or H_2O addition, however, are very similar. CO_2 addition leads to a 18% reduction of the flame velocity in the lean flame and to a 40% reduction in the rich flame velocity. Addition of the same amount of H_2O reduces the flame velocity by 14% in the lean flame and by 25% in the rich one. The larger effects observed in the rich flame result from the procedure adopted to determine the additive initial mole fraction. Keeping constant the ratio $X_{\mathrm{additive}}/X_{CH_4}$ leads to a larger content of the additive in the rich flames.

TABLE 7

Comparison of Measured and Computed Species Mole Fractions in Flame 3b (CH_4–H_2O–air; $\phi = 1.4$)

Mole fractions X at a distance z		Experiment	GRI-Mech 3.0	UCSD	Dagaut	GDFkin®3.0
CH_4	X_i ($z = 0$)	$1.11 \cdot 10^{-1}$	$1.15 \cdot 10^{-1}$	$1.16 \cdot 10^{-1}$	$1.17 \cdot 10^{-1}$	$1.17 \cdot 10^{-1}$
	z ($X_i = X_{i,\mathrm{med}}$), cm	0.12	0.13	0.12	0.10	0.11
O_2	$X_{i,0}$ ($z = 0$)	$1.53 \cdot 10^{-1}$	$1.70 \cdot 10^{-1}$	$1.70 \cdot 10^{-1}$	$1.71 \cdot 10^{-1}$	$1.71 \cdot 10^{-1}$
	$X_{i,f}$ ($z = 0.3$ cm)	$9.41 \cdot 10^{-4}$	$3.09 \cdot 10^{-4}$	$2.33 \cdot 10^{-4}$	$1.30 \cdot 10^{-4}$	$1.56 \cdot 10^{-4}$
	z ($X_i = X_{i,\mathrm{med}}$), cm	0.13	0.14	0.13	0.10	0.11
CO_2	$X_{i,f}$ ($z = 0.3$ cm)	$4.12 \cdot 10^{-2}$	$4.67 \cdot 10^{-2}$	$4.69 \cdot 10^{-2}$	$5.05 \cdot 10^{-2}$	$4.97 \cdot 10^{-2}$
	z ($X_i = X_{i,\mathrm{med}}$), cm	0.15	0.17	0.16	0.12	0.14
H_2O	$X_{i,0}$ ($z = 0$)	$4.45 \cdot 10^{-2}$	$5.35 \cdot 10^{-2}$	$5.28 \cdot 10^{-2}$	$5.09 \cdot 10^{-2}$	$5.16 \cdot 10^{-2}$
	$X_{i,f}$ ($z = 0.3$ cm)	$2.08 \cdot 10^{-1}$	$2.14 \cdot 10^{-1}$	$2.12 \cdot 10^{-1}$	$2.08 \cdot 10^{-1}$	$2.08 \cdot 10^{-1}$
	z ($X_i = X_{i,\mathrm{med}}$), cm	0.12	0.13	0.12	0.10	0.11
CO	$X_{i,f}$ ($z = 0.3$ cm)	$6.38 \cdot 10^{-2}$	$6.25 \cdot 10^{-2}$	$6.39 \cdot 10^{-2}$	$6.11 \cdot 10^{-2}$	$6.23 \cdot 10^{-2}$
	z ($X_i = X_{i,\mathrm{med}}$), cm	0.11	0.13	0.13	0.10	0.10
H_2	$X_{i,f}$ ($z = 0.3$ cm)	$7.08 \cdot 10^{-2}$	$5.91 \cdot 10^{-2}$	$6.17 \cdot 10^{-2}$	$6.46 \cdot 10^{-2}$	$6.49 \cdot 10^{-2}$
	z ($X_i = X_{i,\mathrm{med}}$), cm	0.12	0.13	0.12	0.09	0.10
C_2H_6	$X_{i,\max}$	$1.06 \cdot 10^{-3}$	$1.19 \cdot 10^{-3}$	$1.26 \cdot 10^{-3}$	$1.96 \cdot 10^{-3}$	$2.04 \cdot 10^{-3}$
	z ($X_i = X_{i,\max}$)	0.14	0.15	0.13	0.10	0.12
C_2H_4	$X_{i,\max}$	$1.51 \cdot 10^{-3}$	$1.86 \cdot 10^{-3}$	$2.52 \cdot 10^{-3}$	$2.45 \cdot 10^{-3}$	$2.88 \cdot 10^{-3}$
	z ($X_i = X_{i,\max}$)	0.14	0.16	0.15	0.12	0.13
C_2H_2	$X_{i,\max}$	$2.26 \cdot 10^{-3}$	$1.99 \cdot 10^{-3}$	$1.01 \cdot 10^{-3}$	$1.97 \cdot 10^{-3}$	$2.15 \cdot 10^{-3}$
	z ($X_i = X_{i,\max}$)	0.16	0.20	0.18	0.13	0.15
NO	$X_{i,f}$ ($z = 0.3$ cm)	—	$1.04 \cdot 10^{-5}$	—	—	$3.57 \cdot 10^{-5}$
	z ($X_i = X_{i,\mathrm{med}}$), cm	—	0.2	—	—	0.175

TABLE 8

Influence of CO_2 and H_2O Addition on the Flame Velocity

Kinetic mechanism	Velocity, cm/sec					
	Flame 1a (CH_4–air)	Flame 2a (CH_4–CO_2–air)	Flame 3a (CH_4–H_2O–air)	Flame 1b (CH_4–air)	Flame 2b (CH_4–CO_2–air)	Flame 3b (CH_4–H_2O–air)
	$\phi = 0.7$			$\phi = 1.4$		
GRI-Mech 3.0	18.7	15.1	15.8	14.7	8.5	10.4
Dagaut	17.3	14.2	14.7	22.8	14.2	17.7
UCSD	19.8	16.3	17.3	16	9.7	11.9
GDFkin®3.0	16.8	13.8	14.4	18.7	12.1	14.3

The results (see Tables 9 and 10) show that each additive reduces both the flame velocity and the adiabatic flame temperature for both equivalence ratios. It was worth considering these effects more closely and checking if the decrease in the flame velocity only resulted from a thermal effect or if a chemical effect also contributed. The procedure proposed by Liu et al. [20] was adopted to compare the influence of CO_2 or H_2O and fictitious additives FCO_2 and FH_2O. FCO_2 and FH_2O have the same thermochemical and transport properties as the normal CO_2 and H_2O, respectively, but they are not consumed or produced in the reaction mechanism. They are included in the lists of third-body species with the same collision efficiencies as CO_2 and H_2O, respectively. As the four mechanisms lead to roughly similar results, the following simulation was

TABLE 9

Influence of CO_2 and H_2O on the Flame Velocity and Temperature of Burnt Gases (Lean Methane–Air Flames; $\phi = 0.7$; UCSD Mechanism)

Composition	v_f, cm/sec	T_f, K
$[CO_2]/[CH_4] = 0$	19.8	1 820
$[CO_2]/[CH_4] = 0.4$	16.5	1764
$[FCO_2]/[CH_4] = 0.4$	16.8	1767
$[H_2O]/[CH_4] = 0.4$	17.7	1777
$[FH_2O]/[CH_4] = 0.4$	17.6	1779

TABLE 10

Influence of CO_2 and H_2O on the Flame Velocity and Temperature of Burnt Gases (Rich Methane–Air Flame; $\phi = 1.4$; UCSD Mechanism)

Composition	v_f, cm/sec	T_f, K
$[CO_2]/[CH_4] = 0$	16.0	1983
$[CO_2]/[CH_4] = 0.4$	9.7	1871
$[FCO_2]/[CH_4] = 0.4$	10.1	1882
$[H_2O]/[CH_4] = 0.4$	11.0	1889
$[FH_2O]/[CH_4] = 0.4$	10.5	1887

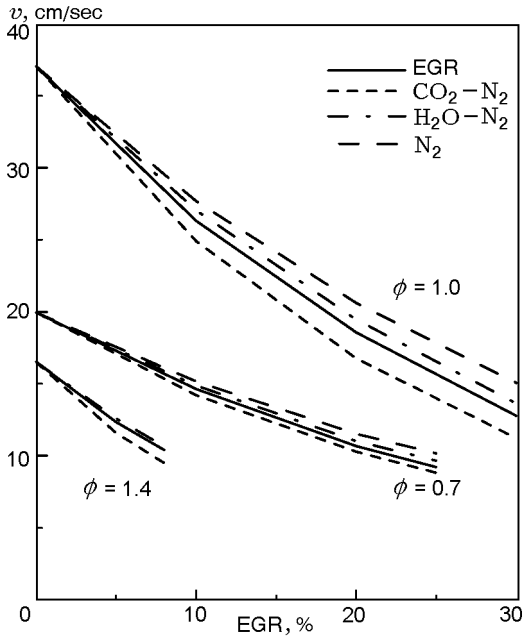

Fig. 3. Influence of exhaust gas recirculation on the flame velocity of lean, stoichiometric, and rich methane–air flames (UCSD mechanism).

performed with the smallest mechanism, UCSD, to reduce the calculations times.

Tables 9 and 10 show that the replacement of CO_2 or H_2O by FCO_2 or FH_2O produces only very minor changes in the flame velocity, especially in the lean flame. Larger changes were reported by Liu et al. [21] who replaced as much as 30% of N_2 contained in air by CO_2 in a numerical study of CH_4 and H_2 flames in a large range of equivalence ratios. In our experimental study, flame stability requirements limited the initial CO_2 or H_2O mole fraction in the unburnt mixture, so that changes in v_f and T_f were also limited.

From a closer examination of the results listed in Tables 9 and 10, however, it can be noticed that the opposite effects are observed for CO_2 and H_2O. Suppressing artificially the chemical reactivity of the additive leads to an increase in the flame velocity for CO_2 and to a decrease in the flame velocity for H_2O. This observation deserves consideration regarding the composition of the burnt gases in EGR simulations. Very often, the burnt gases are assimilated to pure N_2 or to a CO_2–N_2 mixture, whereas, as mentioned in the introduction, H_2O is generally ignored.

Additional UCSD computations performed with stoichiometric, lean ($\phi = 0.7$), and rich ($\phi = 1.4$) CH_4–air flames are summarized in Fig. 3. The objective was to compare, with larger additive concentrations, the changes induced on the flame velocity by addition of N_2 or mixtures composed of CO_2–N_2, H_2O–N_2, and CO_2–H_2O–O_2–N_2. The latter was designed as "EGR," because it was expected to represent the real composition of the burnt gases. In rich and stoichiometric flames, the "EGR" composition was $0.0948\ CO_2 + 0.1896\ H_2O + 0.7156\ N_2$, corresponding to the burnt gases of a stoichiometric flame. In the CO_2–N_2 and H_2O–N_2 binary mixtures, the N_2 mole fraction was kept to 0.7156. In the lean flame, the "EGR" composition was $0.0662\ CO_2 + 0.1338\ H_2O + 0.0604\ O_2 + 0.7396\ N_2$, corresponding to the composition measured at 0.3 cm from the burner surface in the lean methane–air flame (flame 1a). The presence of O_2 was imposed to modify the initial methane–air flame composition to maintain the equivalence ratio at 0.7 in the diluted flame. The EGR added to the lean and the rich flames were limited to 25 and 8%, respectively, to avoid convergence problems encountered with higher EGR contents.

Results show that, for the three equivalence ratios examined, assimilating the exhaust gas to a CO_2–N_2 mixture leads to a lower flame velocity than for the complete EGR (CO_2–H_2O–N_2 mixture). Higher flame velocities are obtained, however, when only N_2 or the H_2O–N_2 mixture is considered. This effect is more pronounced in the stoichiometric flame. Comparing the

slopes of these curves, we can notice that the rich flame is far more sensitive to the recirculation of exhaust gases, followed by the stoichiometric flame, and then the lean one.

The chemical effect of CO_2 on the burning velocity of hydrocarbon–air flames was generally attributed to an increase in the rate of the reaction $CO_2 + H = CO + OH$ [20–22]. This reaction consumes H atoms and reduces the rate of the main branching reaction $H + O_2 = OH + O$. Hence, in addition to its thermal effect, CO_2 produces chemical inhibition. Only few studies concern H_2O addition to hydrocarbon flames, and divergences are observed in the chemical effect exerted on the burning velocity [23–25]. Müller-Dethlefs and Schlader [25] reported, however, that the measured decrease in the flame velocity with steam addition to propane and ethylene flames is smaller than it would be expected in the case with steam acting solely as an inert heat sink. The slight decrease in the flame velocity in the case with H_2O replaced by the fictitious FH_2O (see Tables 9 and 10) is in agreement with this conclusion.

CONCLUSIONS

The main objective of this work was to compare the influence exerted by CO_2 and H_2O addition on the chemical structure of lean and rich methane–air flames. It extended a previous study on CO_2 and H_2 addition to a lean methane–air flame, motivated by the potential use of biogas in gas turbines, toward issues related to the use of EGR to reduce pollutant emissions from combustion systems. As the first step, the chemical structure of lean ($\phi = 0.7$) and rich ($\phi = 1.4$) premixed flames (CH_4–air, CH_4–CO_2–air, and CH_4–H_2O–air) was determined experimentally. The species mole fraction profiles were used to check the accuracy of four reaction mechanisms markedly different in their reactions and species numbers. The four mechanisms reproduce the experimental major species mole fraction profiles reasonably well; however, discrepancies are observed in the prediction of the maximum mole fractions of minor species. Additional flame structure simulations, conducted with fictitious FCO_2 or FH_2O added to methane–air flames, show that, in addition to the main thermal effect, chemical flame inhibition is observed with CO_2, whereas H_2O increases chemically the burning velocity. As N_2 is the main component of the burnt gases, the opposing chemical effects of CO_2 and H_2O are limited in this case. For a more accurate simulation of EGR, however, the presence of H_2O in the burnt gases must be taken into consideration.

REFERENCES

1. S. Ponnusamy, M. D. Checkel, and B. A. Fleck, "Maintaining burning velocity of exhaust-diluted methane–air flames by partial fuel reformation," *IFRF Combust. J.*, No. 200506 (2005).
2. P. Han, M. D. Checkel, B. A. Fleck, and N. L. Nowicki "Burning velocity of methane/diluent mixture with reformer gas addition," *Fuel*, **86**, 585–596 (2007).
3. A. Dubreuil, F. Foucher, C. Mounaïm-Rousselle, G. Dayma, and P. Dagaut, "HCCI combustion: Effect of NO in EGR," *Proc. Combust. Inst.*, **31**, 2879–2886 (2007).
4. J. Y. Ren, W. Qin, F. N. Egolfopoulos, H. Mak, and T. T. Tsotsis "Methane reforming and its potential effect on the efficiency and pollutant emissions of lean methane–air combustion," *Chem. Eng. Sci*, **56**, 1541–1549 (2001).
5. J. Y. Ren, F. N. Egolfopoulos, and T. T. Tsotsis, "NO_x emission control of lean methane–air combustion with addition of methane reforming products," *Combust. Sci. Technol.*, **174**, 181–205 (2002).
6. C. Renard, M. Musik, P. J. Van Tiggelen, and J. Vandooren, "Effect of CO_2 or H_2O addition on hydrocarbon intermediates in rich $C_2H_4/O_2/Ar$ flames," in: *Proc. European Combustion Meeting* (2003).
7. D. Zhao, H. Yamashita, K. Kitagawa, N. Arai, and T. Furuhata, "Behavior and effect on NO_x formation of OH radical in methane–air diffusion flame with steam addition," *Combust. Flame*, **130**, 352–360 (2002).
8. D.-J. Hwang, J.-W. Choi, J. Park, S.-I. Keel, C.-B. Ch, and D.-S. Noh, "Numerical study on flame structure and NO formation in CH_4–O_2–N_2 counterflow diffusion flame diluted with H_2O," *Int. J. Energ. Res.*, **28**, 1255–1267 (2004).
9. J. Biet, J. L. Delfau, L. Pillier, and C. Vovelle, "Influence of CO_2 and H_2 on the chemical structure of a premixed, lean methane–air flame," in: *Proc. European Combustion Meeting* (2007).
10. G. P. Smith, D. M. Golden, M. Frenklach, et al., GRI-Mech 3.0 (1999). http://www.me.berkeley.edu/gri_mech/version30/text30.html.
11. P. Dagaut and A. Nicolle, "Experimental and detailed kinetic modeling study of hydrogen-enriched natural gas blend oxidation over extended temperature and equivalence ratio ranges," *Proc. Combust. Inst.*, **30**, 2631–2638 (2005).
12. University of California, San Diego, Center for Energy Research Combustion Division; http://maemail.ucsd.edu/combustion/cermech/.

13. A. El Bakali, L. Pillier, P. Desgroux, B. Lefort, L. Gasnot, J. F. Pauwels, and I. da Costa, "NO prediction in natural gas flames using GDF-Kin®3.0 mechanism: NCN and HCN contribution to prompt-NO formation," *Fuel*, **85**, 896–909 (2006).
14. J. H. Kent, "A noncatalytic coating for platinum-rhodium thermocouples," *Combust. Flame.*, **14**, 279–282 (1970).
15. J. Biet, J. L. Delfau, A. Seydi, and C. Vovelle, "Experimental and modeling study of lean premixed atmospheric-pressure propane/O_2/N_2 flames," *Combust. Flame*, **142**, 197–209 (2005).
16. U. Bonne, Th. Grewer, and H. Gg. Wagner, "Messungen in der Reaktionzone von wasserstoff-sauerstoff und methane-sauerstoff Flammen," *Z. Phys. Chem.*, **26**, 93–110 (1960).
17. E. W. Kaiser, T. J. Wallington, M. D. Hurley, J. Platz, H. J. Curran, W. J. Pitz, and C. K. Westbrook, "Experimental and modelling study of premixed atmospheric–pressure dimethyl ether–air flames," *J. Phys. Chem.*, **104**, 8194–8206 (2000).
18. R. J. Kee, F. M. Rupley, and J. A. Miller, "CHEMKIN-II: A Fortran chemical kinetics package for the analysis of gas phase chemical kinetics," Sandia National Laboratories Report No. SAND 89-8009B (1989).
19. R. J. Kee, J. F. Grcar, M. D. Smooke, and J. A. Miller, "PREMIX: A Fortran program for modeling laminar one-dimensional premixed flames," Sandia National Laboratories Report No. SAND85-8240 (1985). http://www.ca.sandia.gov/chemkin/.
20. F. Liu, H. Guo, G. J. Smallwood, and O. L. Gülder, "The chemical effects of carbon dioxide as an additive in an ethylene diffusion flame: implications for soot and NO_x formation," *Combust. Flame*, **125**, Nos. 1–2, 778–787 (2001).
21. F. Liu, H. Guo, and G. J. Smallwood "The chemical effect of CO_2 replacement of N_2 in air on the burning velocity of CH_4 and H_2 premixed flames," *Combust. Flame*, **133**, No. 4, P. 495–497 (2003).
22. C. Zhang, A. Atreya, and K. Lee, "Sooting structure of methane counterflow diffusion flames with preheated reactants and dilution by products of combustion," *Proc. Combust. Inst.*, **24**, 1049–1057 (1992).
23. B. S. Babkin and A. V. V'yun, "Effect of water vapor on the normal burning velocity of a methane–air mixture at high pressures," *Combust., Expl., Shock Wave*, **7**, No. 3, 339–341 (1971).
24. I. Fells and A. G. Rutherford, "Burning velocity of methane–air flames," *Combust. Flame*, **13**, 130–138 (1969).
25. K. Müller-Dethlefs and A. F. Schlader, "The effect of steam on flame temperature, burning velocity and carbon formation in hydrocarbon flames," *Combust. Flame*, **27**, 205–215 (1976).